International Journal of Thermal Sciences 151 (2020) 106243

Contents lists available at ScienceDirect

International Journal of Thermal Sciences

journal homepage: http://www.elsevier.com/locate/ijts

Approximate Bayesian computation applied to the identification of thermal damage of biological tissues due to laser irradiation

Bruna R. Loiola [a,b], Helcio R.B. Orlande [b,*], George S. Dulikravich [c]

[a] Department of Mechanical Engineering, Military Institute of Engineering, IME, General Tibúrcio Square, 80, Urca, Rio de Janeiro, RJ, 22290-270, Brazil
[b] Department of Mechanical Engineering, Politécnica/COPPE, Federal University of Rio de Janeiro, UFRJ, Av. Horácio Macedo, 2030, Cidade Universitária, Rio de Janeiro, RJ, 21941-914, Brazil
[c] Department of Mechanical and Materials Engineering, MAIDROC Laboratory, Florida International University, 10555 West Flagler Street, EC 3462, Miami, FL, 33174, USA

ARTICLE INFO

Keywords:
ABC algorithm
Model selection
Parameter estimation
Thermal damage

ABSTRACT

This paper deals with the solution of an inverse bioheat transfer problem, by using Approximate Bayesian Computation (ABC). A Sequential Monte Carlo (SMC) method is applied for simultaneous model selection and model calibration (estimation of the model parameters) by using synthetic measurements. Two competing models are considered in the analysis of the thermal damage of biological tissues. The results show that the ABC-SMC algorithm provides accurate results for the model selection and estimation of the thermal damage model parameters.

1. Introduction

Even though many mathematical equations used to model physical phenomena are based on well-known conservation principles, more than one model can be proposed to represent the physics of a problem. Models can differ by the simplification hypotheses assumed for the conservation principles, their boundary and initial conditions, as well as the selection of required constitutive equations. Moreover, multiple scale phenomena might or might not be considered in the formulation, depending on the sensitivity of the dependent variables of interest for the problem. Besides these situations where the models can be written based on conservation principles and constitutive equations, there are many others that rely on models strongly dependent on the *a priori* information available about the phenomena. Such is especially the case when the models are stochastic, like in biology or economics, for example.

As detailed phenomena in nature are better comprehended, there is a clear trend to develop complex mathematical models, for which accurate predictions can only be obtained if the parameters appearing in the formulation are accurately known. Despite the detailed phenomena included in such models, their results might not be more accurate than simpler models that are better parameterized, based on the principle of parsimony [1]. The main issue is the reliability and the realism of the computational results obtained with possibly different models. Therefore, techniques for the selection of the most appropriate model to represent the phenomena of interest, as well as for the estimation of the parameters associated with this model, are of great interest for several current practical applications.

Classical information criteria are available for model selection, such as the Akaike Information Criterion (AIC) [2] and the Bayesian Information Criterion (BIC) [3]. Similarly, many techniques have been developed in the past for the estimation of model parameters, from the measured and computational response of the system of interest, through inverse analyses [1,4–30]. An article by Farrell et al. [31] presents a comprehensive approach for model selection, calibration and validation within the Bayesian framework. On the other hand, there are situations where the likelihood is not exactly known, analytically intractable or when the computational cost of the actual likelihood is prohibitive. For such cases, the so-called Approximate Bayesian Computation (ABC) has been developed, where the likelihood is not computed to quantify the mismatch between the computational and the experimental dependent variables of the problem [32–37].

The Approximate Bayesian Computation algorithm of Toni et al. [34] is used in this work for simultaneous model selection and model calibration (estimation of the model parameters) for an inverse bioheat transfer problem [38,39]. Two competing models are considered for the thermal damage of a biological tissue during thermal ablation imposed by a laser, namely: (1) Arrhenius formulation [40,44] and (2) Two-state model [44,45]. In order to verify the Approximate Bayesian

* Corresponding author.
E-mail addresses: bruna.loiola@ime.eb.br (B.R. Loiola), helcio@mecanica.coppe.ufrj.br (H.R.B. Orlande), dulikrav@fiu.edu (G.S. Dulikravich).

https://doi.org/10.1016/j.ijthermalsci.2019.106243
Received 8 April 2019; Received in revised form 22 December 2019; Accepted 23 December 2019
Available online 9 January 2020
1290-0729/

Nomenclature

c_p	specific heat at constant pressure, J/(kg K)
E_a	activation energy, J/mol
g	anisotropy coefficient
h	specific enthalpy, J/kg
h_∞	heat transfer coefficient, W/(m^2 K)
h_{fg}	latent heat, J/kg
H	height of the geometry, m
k	thermal conductivity, W/(m K)
m_f	mass fraction of fat
m_p	mass fraction of protein
m_w	mass fraction of water
$\mathbf{M}$	vector that indexes the models
$\mathbf{P}$	vector of model parameters
P_l	laser power, W
$\dot{Q}$	heat source per unit volume, W/m^3
r, z	spatial coordinates
R	radius of the geometry, m
R_u	universal gas constant, J/(mol K)
S	fraction of surviving cells
t	time
T	temperature, °C
T_∞	surrounding environment temperature, °C
$\mathbf{Y}$	vector of measurements

Greek Symbols

α	parameter of the two-state model, s^{-1}
β	parameter of the two-state model
γ	parameter of the two-state model, K
$\boldsymbol{\varepsilon}$	vector of tolerances
κ	frequency factor exponent
μ_a	radiation absorption coefficient, m^{-1}
μ_{eff}	radiation attenuation coefficient, m^{-1}
μ_s	radiation scattering coefficient, m^{-1}
ρ	density, kg/m^3
σ	laser spot half radius, m
ϕ_0	maximum flux at the laser beam center, W/m^2
ω	perfusion coefficient, $m_b^3 s^{-1} m_t^{-3}$
Ω	thermal damage integral

Subscripts

0	initial time
b	blood
l	laser
m	metabolism

Superscripts

–	refers to tissue properties before phase change
+	refers to tissue properties after phase change

Computation algorithm of Toni et al. [34], non-intrusive synthetic measurements of the tissue damage are used in the inverse analysis. Modeling thermal damage of tissues is an open subject in the literature, since different models are available and values reported for the model parameters exhibit large variability (see, for example [40–45]). Therefore, robust and powerful techniques are urgently needed for model selection and model calibration in the study of the thermal damage of tissues. This is especially the case for the hyperthermia treatment of cancer, with the use of nanoparticles for selective heating of the tumor and control of the heating process to avoid damage of the healthy cells [46].

2. Physical problem and mathematical models

The physical problem considered here involves the laser heating of a biological tissue composed of 65%wt of water and 35%wt of protein, as in Loiola et al. [38]. The tissue consists of a cylindrical geometry, with 3 mm of radius and 3 mm of height. Initially, the tissue is assumed at the uniform body temperature, T_b. A laser heating is then applied at the surface of the tissue at $z = H$, while the boundaries at $r = R$ and $z = 0$ remain at the body temperature, T_b. The boundary at $z = H$ also exchanges heat by convection and linearized radiation with the surrounding environment at the temperature T_∞, with a heat transfer

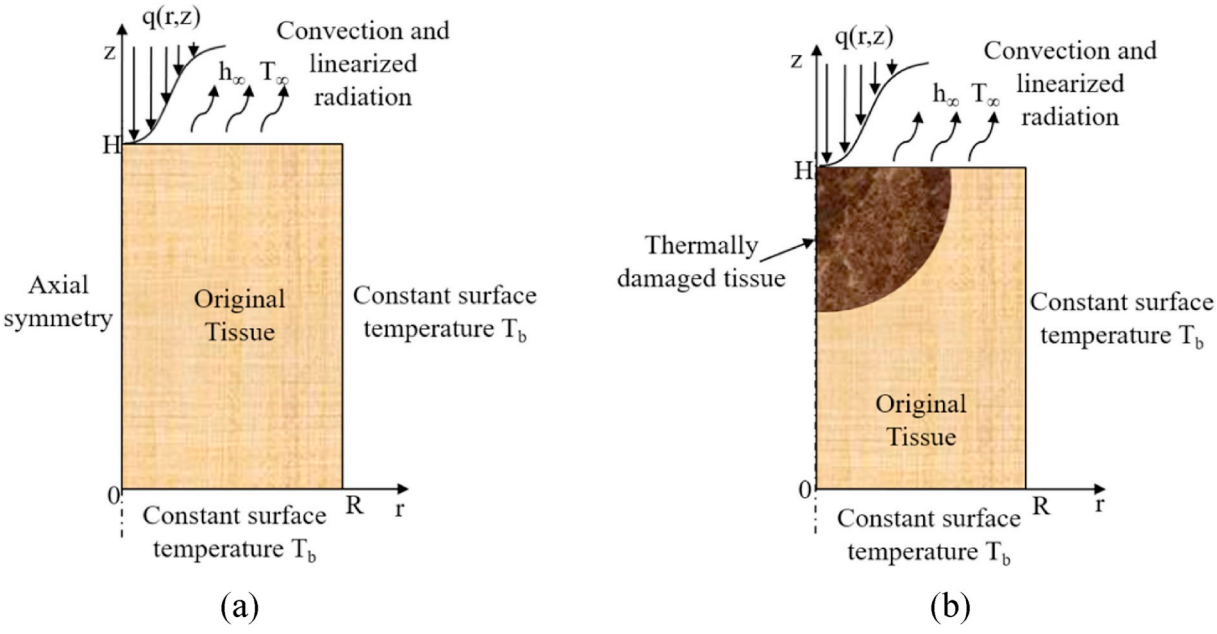

Fig. 1. Laser heating of a biological tissue.

coefficient h_∞. Fig. 1 illustrates the axisymmetric physical problem when the domain contains only the original homogeneous tissue (a) and when part of the tissue has been thermally damaged due to the laser heating (b).

The mathematical formulation for this physical problem is given by:

$$\rho(r,z)\frac{\partial h(r,z,t)}{\partial t}=\nabla\cdot[k(r,z)\nabla T(r,z,t)]+\dot{Q}(r,z)\quad 0<r<R,\quad 0<z<H,\quad t>0 \tag{1a}$$

$$T(r,z,t)=T_b \qquad 0<r<R,\quad 0<z<H,\quad t=0 \tag{1b}$$

$$\frac{\partial T(r,z,t)}{\partial r}=0 \qquad r=0,\quad 0<z<H,\quad t>0 \tag{1c}$$

$$T(r,z,t)=T_b \qquad r=R,\quad 0<z<H,\quad t>0 \tag{1d}$$

$$T(r,z,t)=T_b \qquad 0<r<R,\quad z=0,\quad t>0 \tag{1e}$$

$$-k(r,z)\frac{\partial T(r,z,t)}{\partial z}=h_\infty(T-T_\infty) \qquad 0<r<R,\quad z=H,\quad t>0 \tag{1f}$$

The enthalpy form for the bioheat transfer equation, proposed by Abraham and Sparrow [39], is used in this work to account for the water phase change inside the tissue. The enthalpy is related to the temperature by Ref. [39]:

$$h=\begin{cases}\left[c_p(r,z)\right]_t^-[T(r,z,t)-T_b] & T\le 99^\circ C\\ h(99)+h_{fg}m_w\dfrac{[T(r,z,t)-99]}{(100-99)} & 99^\circ C<T\le 100^\circ C\\ h(100)+\left[c_p(r,z)\right]_t^+[T(r,z,t)-100] & T>100^\circ C\end{cases} \tag{2}$$

The thermal properties density (ρ), specific heat (c_p) and thermal conductivity (k) are considered as functions of the tissue composition, which are related to the mass content of water (m_w), protein (m_p) and fat (m_f), as proposed by Cooper and Trezek [47]:

$$\rho=\frac{1}{m_w+0.649m_p+1.227m_f} \qquad [g/cm^3] \tag{3}$$

$$c_p=4.2m_w+1.09m_p+2.3m_f \qquad [J/(g^\circ C)] \tag{4}$$

$$k=\rho\left(6.28m_w+1.17m_p+2.31m_f\right) \qquad [mW/(cm\,K)] \tag{5}$$

The source term in Eq. (1a) includes the energy supplied by blood perfusion, tissue metabolism and the heating laser, that is:

$$\dot{Q}(r,z)=\dot{Q}_b(r,z,\Omega)+\dot{Q}_m(\Omega)+\dot{Q}_l(r,z) \tag{6}$$

The blood perfusion source term is taken as [48]:

$$\dot{Q}_b(r,z,\Omega)=\rho_b c_b\omega_b(\Omega)[T_b-T(r,z)] \tag{7}$$

where T_b represents the arterial blood temperature, ρ_b the density and c_b the specific heat of the blood. The perfusion coefficient ω_b is considered as a function of the tissue thermal damage, Ω [39]:

$$\omega_b=\begin{cases}\left(1+25\,\Omega-260\,\Omega^2\right)\omega_0 & \Omega\le 0.1\\ (1-\Omega)\omega_0 & 0.1<\Omega\le 1\\ 0 & \Omega>1\end{cases} \tag{8}$$

where ω_0 is the blood perfusion of the healthy tissue. Values of thermal damage up to $\Omega = 0.1$ increase the perfusion due to vasodilation of the heated tissue, while values of thermal damage in $0.1 < \Omega \le 1$ decrease the blood perfusion due to blood clotting. The value of Ω equal to unity ($\Omega = 1$) is associated with blood coagulation and tissue necrosis, when perfusion is then ceased ($\omega_b = 0$) [39]. The correlations given by Eq. (8) were used by Abraham and Sparrow [39], based on the experimental works of Henriques and Moritz [40–43].

The term $\dot{Q}_m(\Omega)$ in Eq. (6) corresponds to the metabolic heat generation, which was considered uniform in the original homogeneous tissue. On the other hand, the metabolic heat generation is null when the tissue becomes necrotic ($\Omega = 1$) due to the thermal damage.

The energy provided by the laser is modeled with Beer-Lambert's law, due to the small size of the region considered in this work [49]. The laser beam applied at $z = H$ is Gaussian, with radius 2σ, fluence ϕ_0 and attenuation coefficient μ_{eff}, so that,

$$\dot{Q}_l(r,z)=\mu_{eff}\phi_0\exp\left[-\mu_{eff}(H-z)\right]\exp\left(-\frac{r^2}{2\sigma^2}\right) \tag{9}$$

The laser fluence is given by Ref. [50]:

$$\phi_0=\frac{P_l}{2\pi\sigma^2} \tag{10}$$

while the attenuation coefficient is calculated with the absorption (μ_a), scattering (μ_s) and anisotropy (g) coefficients, that is [51]:

$$\mu_{eff}=\{3\mu_a[\mu_a+\mu_s(1-g)]\}^{0.5} \tag{11}$$

Two different models are used here to predict the thermal damage resulting from the laser heating, namely, an Arrhenius model (Model 1) and a two-state model (Model 2). The Arrhenius model for the thermal damage was first proposed by Henriques and Moritz [40–43] and considers that the necrosis of the tissue occurs when $\Omega = 1$. The Arrhenius formulation is given by Eq. (12) and relates the damage of the tissue to the temperature (T) and time (t) of heating. The parameters of Model 1 are the universal gas constant (R_u), activation energy, E_a, and frequency factor, which is expressed here in power form, that is, 10^κ.

$$\Omega=\int_0^t 10^\kappa\exp\left(-\frac{E_a}{R_uT}\right)dt \tag{12}$$

The two-state model (Model 2) was derived by Feng et al. [45] with a thermodynamic analysis related to the fraction of surviving cells (S). The authors performed *in vitro* experiments and correlated the fraction of surviving cells with the temperature and time of heating, by using three parameters: α, β and γ. The two-state model is given by:

$$S(t,T)=\frac{1}{1+\exp\left[-\left(\frac{\gamma}{T}-\beta-\alpha t\right)\right]} \tag{13}$$

The tissue thermal damage is related to the fraction of surviving cells in the two -state model by Ref. [49]:

$$\Omega=\ln\left\{\frac{S(0)}{S(t)}\right\} \tag{14}$$

These two competing models will be considered to represent the synthetic experimental data. Model selection and model calibration with an ABC-SMC algorithm is presented in the next section.

3. Model selection and model calibration

Approximate Bayesian Computation (ABC) is used in this work for simultaneous model selection and estimation of the model parameters (calibration). Methods of this class can deal with experimental uncertainties that may not be appropriately modeled in terms of analytic statistical distributions or the computation of the likelihood function is very time consuming [34,35,52–54].

The algorithm of Toni et al. [34], which is an extension of the Sequential Monte Carlo algorithm of Sisson et al. [33], is used here for model selection and model calibration. Therefore, the present objective is to obtain the combined posterior distribution, $\pi(\mathbf{P},\mathbf{M}|\mathbf{Y})$, where $\mathbf{M}$ is the vector that indexes the models that are considered in the analysis, $\mathbf{P}$ is the vector of model parameters and $\mathbf{Y}$ is the vector of measurements. In this algorithm, a model is initially selected from the prior $\pi(\mathbf{M})$, and then a sample for the parameters of this model is obtained from their prior distributions. This process of selecting the model and sampling the

parameters is repeated until a pre-specified number of samples (N) are accepted. A user-selected distance function, $d(\mathbf{Y},\mathbf{Y}^*)$, between measurements ($\mathbf{Y}$) and estimated dependent variables ($\mathbf{Y}^*$), is used as the acceptance criterion instead of the likelihood, with a specified tolerance (ε), that is, $d(\mathbf{Y},\mathbf{Y}^*) \leq \varepsilon$. The set of accepted particles is named population. Weights are calculated for each particle and normalized according to each model. New populations of size N are then generated by sampling the model from its prior and sampling the model parameters from their values at the previous population. This process is repeated until the tolerance for the last population, ε_P, is satisfied, where P indicates the number of populations. Tolerances are usually set large for the first populations, in order to avoid lack of convergence when the sampling is dominated by the priors. The information provided by the measurements becomes more significant as the populations advance. Consequently, a larger number of particles is selected for the correct model and the samples for the parameters better reflect the real posterior distribution. Convergence tolerances are then gradually reduced for accurate model selection and parameter estimation as the populations advance.

The ABC algorithm of Toni et al. [34] used in this work is summarized by Table 1.

4. Results and discussions

In order to generate the synthetic measurements, the temperature field was computed with the finite volume method [55,56] by using the explicit enthalpy scheme, on a mesh with 245 vol in radial and longitudinal directions and a time step of 0.2 ms. Verification and validation of this finite volume code for the solution of the direct problem were presented by Loiola et al. [38]. The numerical codes were implemented in MATLAB® and run on a computer with processor Intel® Core™i7-7500U CPU@2.70Ghz, with 16 Gb of RAM. The ABC code took around 170 h to reach the convergence for each test. The properties of the blood and tissue, as well as the heat source parameters used to generate the synthetic measurements, are presented by Table 2. The values of parameters of the two thermal damage competing models (Model 1 - Eq. (12) and Model 2 - Eqs. (13) and (14)) for PC-3 prostate cancer cells, which were used in this work, are presented by Table 3 [45].

A sensitivity analysis was performed by sampling one parameter at a time from its prior distribution (see Table 4) and simulating the forward problem. Each parameter was sampled one hundred times. The priors were supposed as uniform distributions with large variances, which encompass the reported parameter values for different cell lines. The curves obtained with each simulation are presented by Figs. 2 and 3. Fig. 2 present the results for the transient variation of temperature at three different radial positions over the heated surface ($z = H$). Fig. 3 present the results obtained for the thermal damage (Ω) over this same surface, at the radial position $r = 0.75$ mm. The behaviors of the thermal damage for other radial positions are similar to those presented by Fig. 3 and are omitted here for the sake of brevity. The curves obtained by sampling the parameters of model 1 are presented by Figs. 2a and 3a (parameter κ), and Figs. 2b and 3b (parameter E_a). Similarly, the curves obtained by sampling the parameters of model 2 are presented by Figs. 2c and 3c (parameter α), Figs. 2d and 3d (parameter β) and Figs. 2e and 3e (parameter γ).

As can be observed at Fig. 2, the temperature at the heated surface has no sensitivity with respect to variations of the damage parameters, either for model 1 or model 2, since the curves obtained with one hundred samples are superimposed at the graph scale. Moreover, the temperature variations obtained with models 1 and 2 are the same. Therefore, temperature measurements cannot be used to estimate the model and its associated parameters related to the decomposition of the tissue, because of low sensitivity. On the other hand, the thermal damage is very sensitive to variations in the parameters of models 1 and 2, except for α, as shown by Fig. 3. Based on the analysis of Figs. 2 and 3, the inverse problem was solved with non-intrusive transient measurements of the necrosis front position at the surface heated by the laser. The interface between decomposed and original tissues was considered as the point where $\Omega = 1$ (necrosis front). Measurements of the necrosis front position can be obtained in practice with optical observations of the tissue color changes [61,62].

The reduced sensitivity coefficients [1,24,25,30] of the thermal damage front with respect to the different parameters are presented in Fig. 4a and b, for models 1 and 2, respectively. The reduced sensitivity coefficients were calculated with the parameter values given in Table 3. They are obtained by multiplying the sensitivity coefficients by the values of the corresponding parameters [1,15–26]. Fig. 4a and b shows that the sensitivity coefficients are null for small times, while necrosis has not yet developed over the heated surface. The sensitivity coefficients for parameters κ and E_a of model 1, as well for parameters β and γ of model 2, suddenly increase when necrosis starts and then decay to steady-state values. The sensitivity coefficient with respect to the

Table 1
ABC algorithm [34].

1. Define the tolerances ε_1, ε_2, …ε_P for each of the iterations (populations) used for selecting the model and its parameters. Also, specify the distance function $d(\mathbf{Y},\mathbf{Y}^*)$ that substitutes the likelihood function. Set the population indicator $p = 0$.
2. Set the particle indicator $i = 1$, where each particle represents, at each iteration, a model and its parameters.
3. Sample the model M^* from the prior distribution for the models $\pi(\mathbf{M})$.
If $p = 0$, sample the candidate parameters $\mathbf{P}^{**}$ from the prior distribution for the parameters of model M^*, that is, $\pi[\mathbf{P}(M^*)]$. Else, sample $\mathbf{P}^*$ from the parameters in the previous population $P(M^*)^i_{p-1}$, with weights $w(M^*)^i_{p-1}$, and perturb this particle to obtain $\mathbf{P}^{**} \approx K_p(\mathbf{P}^*, \mathbf{P}^{**})$, where K_p is a perturbation kernel.
4. If $\pi(\mathbf{P}^{**}) = 0$, return to step 3. Else, simulate from the forward problem (operator f) a candidate set of observable variables with model M^* and parameters $\mathbf{P}^{**}$, that is, $\mathbf{Y}^* = f(\mathbf{Y}|\mathbf{P}^{**}, M^*)$.
5. If $d(\mathbf{Y},\mathbf{Y}^*) > \varepsilon_p$, return to step 3. Otherwise, set $M^i_p = M^*$, add $\mathbf{P}^{**}$ to the population of particles $P(M^*)^i_p$ and calculate the particle weight

$$w(M^*)^i_p = \begin{cases} 1 & \text{if } p = 0 \\ \dfrac{\pi(P(M^*)^i_p)}{\sum_{j=1}^{N} w(M^*)^j_{p-1} K_p(P(M^*)^j_{p-1}, P(M^*)^i_p)} & \text{if } p > 0 \end{cases}$$

6. If $i < N$, where N is the number of particles, set $i = i + 1$ and go to step 3.
7. Normalize the weights.
8. If $p < P$, where P is the number of iterations (populations), set $p = p + 1$ and go to step 2. Otherwise, terminate the iterations.

Table 2
Biological and blood properties and heat source parameters.

Parameter	Value	Unit	Reference
ρ^-	1140	kg/m^3	[47]
ρ^+	4400	kg/m^3	[47]
c_p^-	3110	J/(kg K)	[47]
c_p^+	382	J/(kg K)	[47]
k^-	0.512	W/(m K)	[47]
k^+	0.180	W/(m K)	[47]
ρ_b	1000	kg/m^3	[39]
c_b	4100	J/(kg K)	[39]
ω_0	0.0028	$m_b^3 s^{-1} m_t^{-3}$	[39]
T_b	37	°C	[39]
h_{fg}	2257000	J/kg	[57]
m_w	0.65	–	[38]
m_p	0.35	–	[38]
$\dot{Q}_m$	170	W/m^3	[39]
μ_{eff}	4060	m^{-1}	[58]
h_∞	10	W/(m^2 K)	[59]
T_∞	25	°C	[59]
P_l	10	W	[60]
σ	0.5	mm	[60]
ϕ_0	636.62	W/cm^2	[50]
R	0.003	m	–
H	0.003	m	–

Table 3
Exact values of the parameters for the competing thermal damage models.

Model	Parameter	Value [45]
1	κ	35
	E_a [kJ/mol]	231.8
2	α [s^{-1}]	0.0049
	β	215.64
	γ [K]	70031

Table 4
Priors for the parameters of each model.

Model	Parameter	Prior	Reference
1	κ	U(20,130)	[61]
	E_a [kJ/mol]	U(200,800)	
2	α [s^{-1}]	U(0.001,0.010)	[45]
	β	U(150,300)	
	γ [K]	U(60000,80000)	

parameter α of model 2 is null, as also revealed by the sensitivity analysis presented by Fig. 3c. The sensitivity coefficients are not linearly dependent for the parameters of model 1, except when they reach steady state values. On the other hand, parameters β and γ of model 2 are correlated, as shown by Fig. 4b.

For the results presented below, the synthetic transient measurements of the necrosis front were assumed available with a frequency of 100 Hz. The synthetic measurements were Gaussian, with means given by the solution of the direct problem and standard deviations of 1% of these mean values. In order to avoid an inverse crime, the inverse problem was solved on a mesh much coarser than that used to generate the synthetic measurements (163 control volumes in each direction and a time step of 0.2 ms). The duration of the simulated experiments was taken as 0.187 s.

The uniform transition kernels presented by Table 5 were used to generate the particles for the parameters in step 3 of the algorithm of Toni et al. [34], and the two competing models were assumed as equally probable to represent the measured data. Eleven populations of this algorithm, with 1000 particles each, were used in this work for the solution of the inverse problem. These numbers of populations and particles, as well as the tolerances for the convergence of each population, were selected based on numerical experiments.

The function used in step 5 of the algorithm of Toni et al. [34] (see Table 1), in order to verify the agreement between the measurements $\mathbf{Y}$ and the estimated responses $\mathbf{Y}^*$, was the Euclidean distance between these two vectors. The convergence tolerances were gradually reduced as the populations advanced, and the tolerance for the final population was set based on Morozov's discrepancy principle [7]. The following vector of tolerances $\boldsymbol{\varepsilon} = [4.2 \times 10^{-3}, 1.1 \times 10^{-3}, 8.5 \times 10^{-4}, 6.8 \times 10^{-4}, 4.7 \times 10^{-4}, 3.8 \times 10^{-4}, 3.0 \times 10^{-4}, 2.1 \times 10^{-4}, 1.3 \times 10^{-4}, 8.5 \times 10^{-5}, 6.4 \times 10^{-5}]$ m was used as the convergence criterion. For each test-case examined in this work, the inverse problem was solved at least four times, with different sets of synthetic measurements, in order to examine possible discrepancies in the obtained results. The inverse problem solution was not sensitive to the set of synthetic measurements and the results of one single run of the algorithm of Toni et al. [34] are presented below.

We consider first a case where the synthetic measurements were generated with model 1. Fig. 5 presents the numbers of particles selected for each model as the populations evolved. This figure shows that model 1 was correctly the only one selected from population 8 onwards. Despite that the correct model has been the only one selected at population 8, additional populations were required to improve the calibration of the model parameters.

The histogram of the parameters for model 1 at the final population are shown by Fig. 6. The histograms for the two parameters of model 1 exhibit small variances, despite the large intervals initially assigned by their uniform priors (see Table 4). The mean values for each parameter and their 95% credibility intervals (obtained from the 2.5% and 97.5% quantiles) are given by Table 6. Although these estimated mean values are quite different from the exact ones used to generate the synthetic measurements (see Table 3), the agreement between estimated and measured transient positions of the necrosis front is very good. Such a fact is demonstrated by Fig. 7, which presents the synthetic measurements and the transient front positions estimated with the mean values of the parameters given by Table 6. Fig. 7 shows that the estimated front agrees with the measurements within their related uncertainties.

For the case examined above, the ABC algorithm of Toni et al. [34] was capable of selecting the correct model, but the estimated mean parameters were quite far from the exact values used to generate the synthetic measurements. Therefore, these results reveal that multiple sets of parameters can represent the measured data with model 1, within the uniform priors with large variances used for this case (see Table 4). On the other hand, the ABC algorithm can simultaneously select the model and estimate the correct parameter values if priors with smaller variances are used for the model parameters. In order to illustrate this behavior, we now consider a case in which the priors for the parameters of model 1 are given by U(20,50) and U(200,250) kJ/mol for κ and E_a, respectively, instead of those presented by Table 4. For this case, the priors for the parameters of model 2 are still given by Table 4 and the two models are considered equally probable. Such as for the case above, model 1, which was used to generate the synthetic measurements, was correctly the only one selected from population 8 onwards. The statistics obtained for the parameters of model 1 at the final population are presented by Table 7. This table shows that the estimated means are now in excellent agreement with the values used to generate the synthetic measurements (see Table 3) and that the estimated parameters exhibit small variances. As expected, the agreement between synthetic measurements and the necrosis front positions obtained with the mean parameter values is excellent, as revealed by Fig. 8.

Figs. 7 and 8 reveal that values reported in the literature for the parameters of model 1 need to be used with great caution, since different sets of parameter values may result with the same qualitative thermal damage. However, an analysis of the residuals can provide additional information regarding which set of parameter values is more appropriate to represent the measured data [1,8,25,30]. Residuals are defined by the difference between the measurements and the dependent variables simulated with the selected model and the estimated parameters. Residuals are expected to be small and with a random behavior, if the model selection and model calibration are adequate. Otherwise, if the residuals are large or exhibit a specific trend (signature), either the model or the parameter values do not appropriately represent the measured data [1,8,25,30]. Fig. 9 presents the residuals for the results of Figs. 7 and 8, that is, for the synthetic measurements generated with model 1 and the parameter priors with large and small variances, respectively. Although Approximate Bayesian Computation does not rely on the actual modeling of the measurement errors, since the likelihood is not used for the model selection/calibration, Fig. 9 shows that the residuals obtained with the priors with small variances (see also Table 7 and Fig. 8) are small and exhibit a random behavior centered at the null value. On the other hand, the residuals obtained with the priors with large variances (see also Table 6 and Fig. 7), which resulted in estimated parameters quite different from the exact ones, clearly increase from negative to positive values as time increases. The uncorrelated behavior of the residuals obtained with the priors with small variances indicate that the model selection/calibration was appropriate for this case, as opposed to the correlated residuals obtained with priors with large variances.

The ABC-SMC algorithm of Toni et al. [34] naturally provides a framework for uncertainty quantification of the inverse problem solution, since the particles at the final population represent samples of the approximate posterior distribution for the model parameters. These

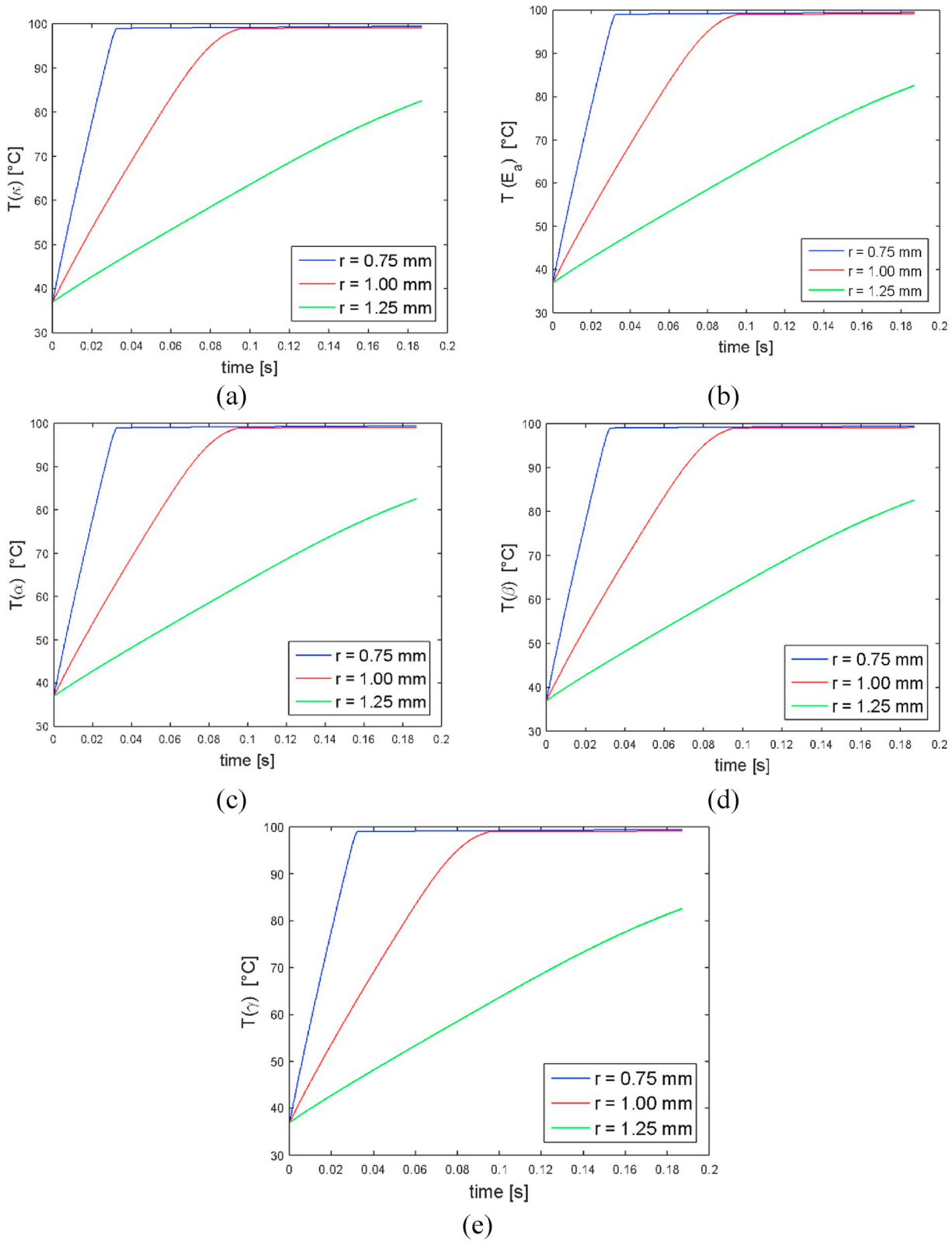

Fig. 2. Temperature variation at the heated surface ($z = H$) for three distinct radial positions by sampling the thermal damage parameters. Model 1: (a) κ; (b) E_a; Model 2: (c) α; (d) β; (e) γ.

samples were then used here to compute the necrosis front position inside the domain at the final time. The 1000 front positions computed with model 1, by using the parameter values given by each of the particles at the final population of the algorithm, are shown by the light blue lines in Fig. 10. These curves were obtained for the case with small variances in the prior. The exact necrosis front, obtained with the parameter values given by Table 3 for model 1, is also shown in this figure. Fig. 10 reveals that the front position at the final time has a small variance and that the exact position falls within the related uncertainties of the numerical simulations.

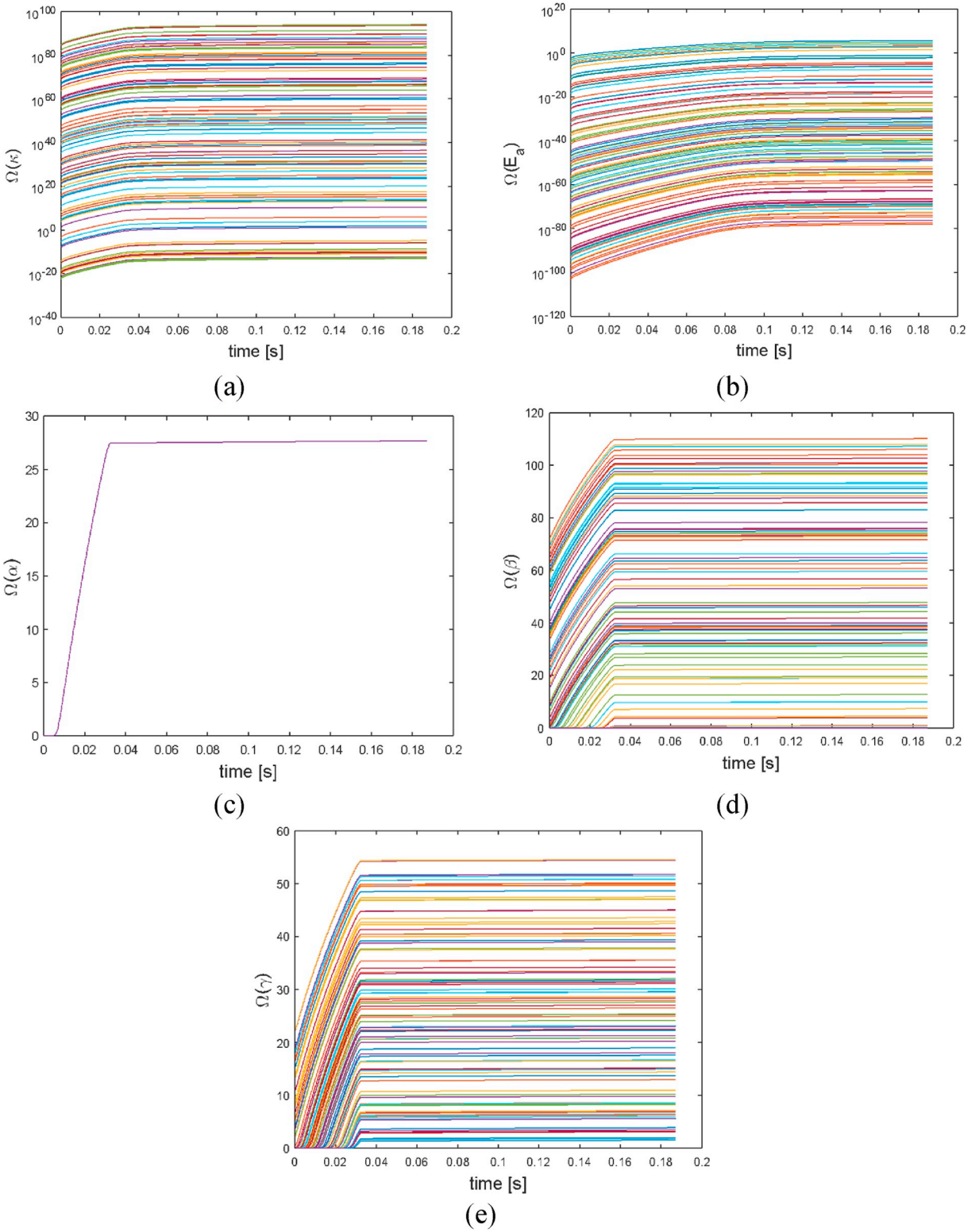

Fig. 3. Thermal damage variation at the heated surface ($z = H$) for $r = 0.75$ mm by sampling the thermal damage parameters. Model 1: (a) κ; (b) E_a; Model 2: (c) α; (d) β; (e) γ.

We now consider a case where the synthetic measurements were obtained with model 2, using the parameter values presented by Table 3. For the results presented below, the priors are given by Table 4. Such as for the cases presented above, the ABC-SMC algorithm of Toni et al. [34] is capable of selecting the correct model in few populations, as shown by Fig. 11. The histograms of the model parameters at the final population, presented by Fig. 12, exhibit Gaussian behaviors, centered at mean values quite close to the exact parameter values and with small variances. This behavior is different from that observed with the other cases where the measurements were obtained with model 1. The means and 95% credibility intervals for the estimated parameters of model 2 are presented by Table 8.

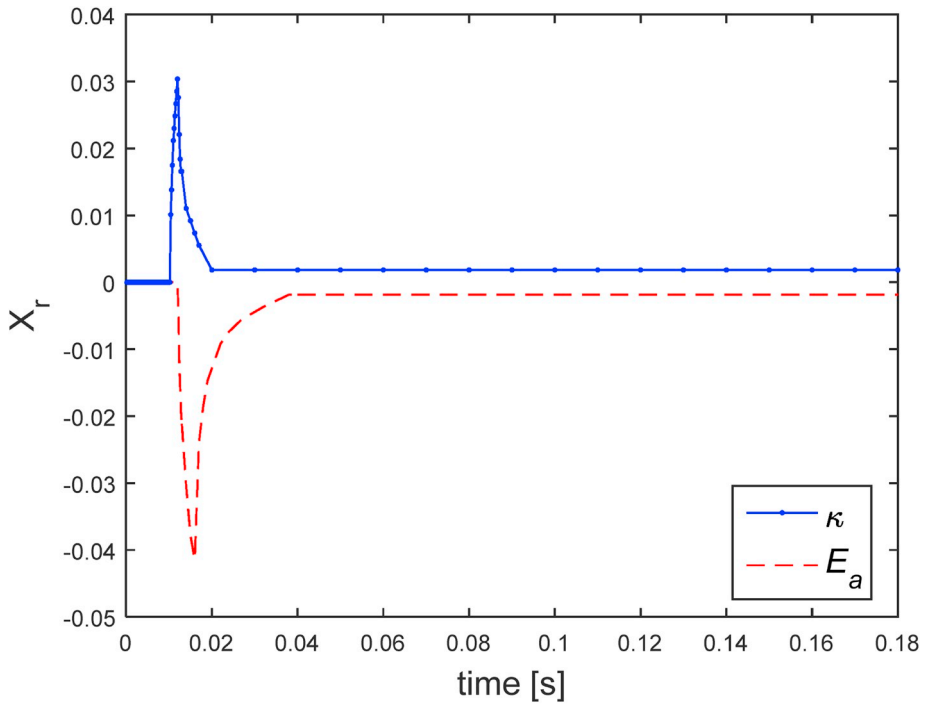

(a)

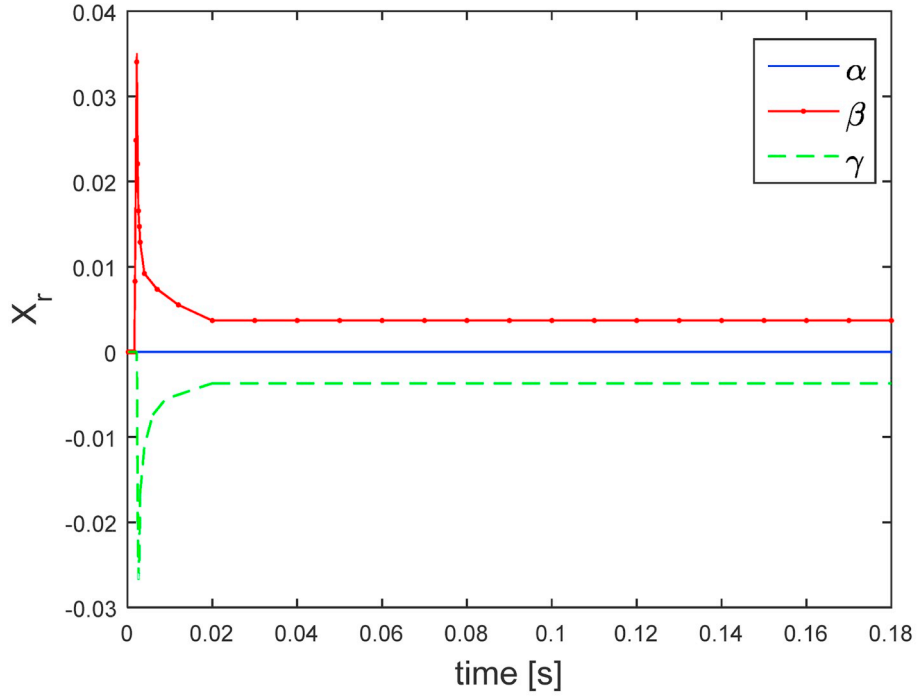

(b)

Fig. 4. Reduced sensitivity coefficients for the parameters of. model 1 (a) and model 2 (b).

The comparison between the measurements and the estimated transient necrosis front, which was obtained with the mean parameter values given by Table 8, is presented by Fig. 13 for the present case. An analysis of this figure reveals an excellent agreement between the estimated transient front positions and the measurements. The residuals for this case are not presented here for the sake of brevity, but they are small and uncorrelated. The simulation under uncertainty of the front position at the final time, which was obtained with the parameter values corresponding to the particles at the final population of the algorithm, is presented by Fig. 14. This figure shows that the exact necrosis front at

Table 5
Transition kernels for the parameters of each model.

Model	Parameter	Transition Kernel
1	κ	U(-3,3)
	E_a [kJ/mol]	U(-10,10)
2	α [s^{-1}]	U(-0.001,0.001)
	β	U(-3,3)
	γ [K]	U(-500,500)

the final time falls within the curves obtained with the particles for the parameters of model 2. These 1000 curves exhibit small variances.

The inverse analysis of model selection and model calibration of thermal damage to tissues was also performed with synthetic intrusive measurements of the necrosis front at the final time. However, the algorithm developed by Toni et al. [34], which was used in this work, was not capable of selecting the model used to generate the synthetic measurements in this case, and final populations exhibited particles of both models.

5. Conclusions

The method used for the simultaneous model selection and parameter estimation of the thermal damage in heating processes of biological tissues was the algorithm of Approximate Bayesian Computation (ABC) developed by Toni et al. [34]. The case considered here involved the heating of a biological tissue with 65% of water and 35% of protein, with a laser of 10 W of power and 2 mm of beam diameter. In order to avoid an inverse crime, the solution of the inverse problem was obtained with a mesh less refined than that used to generate the synthetic measurements. Two models of thermal damage were analyzed: Arrhenius formulation and two-state model.

A sensitivity analysis revealed that the temperature at the heated surface is not affected by the models examined in this work and by their parameters. Therefore, the simulations were performed considering synthetic non-intrusive measurements of the transient position of the necrosis front at the heated surface. The synthetic measurements were generated with either one of the two models, with reference values for the parameters obtained from the literature for PC-3 prostate cancer cells. The measurements were Gaussian, with zero means and standard

Table 6
Statistics for the parameters of model 1 – measurements generated with model 1.

Parameters	Mean	Standard deviation	Quantile 2.5%	Quantile 97.5%
κ	82.3	0.3	81.9	82.8
E_a [kJ/mol]	566	2	562	568

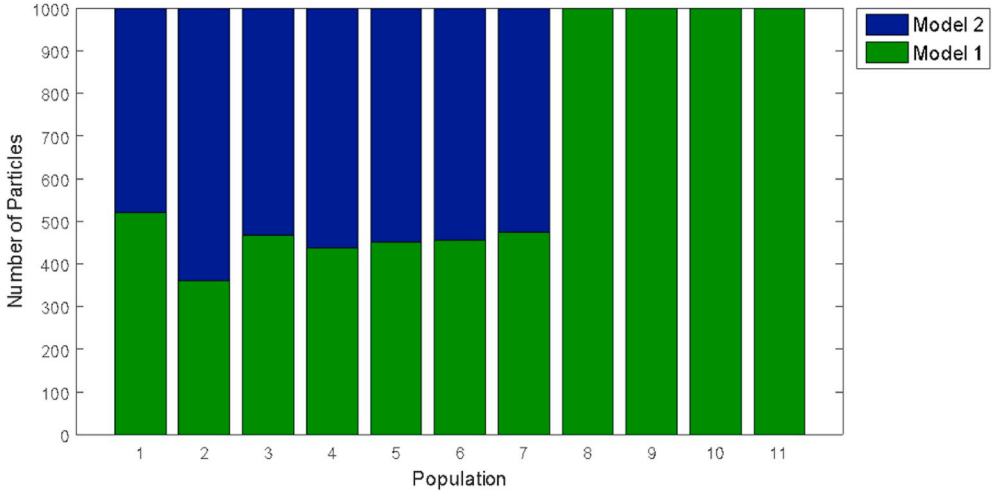

Fig. 5. Number of accepted particles at each population –. measurements generated with model 1.

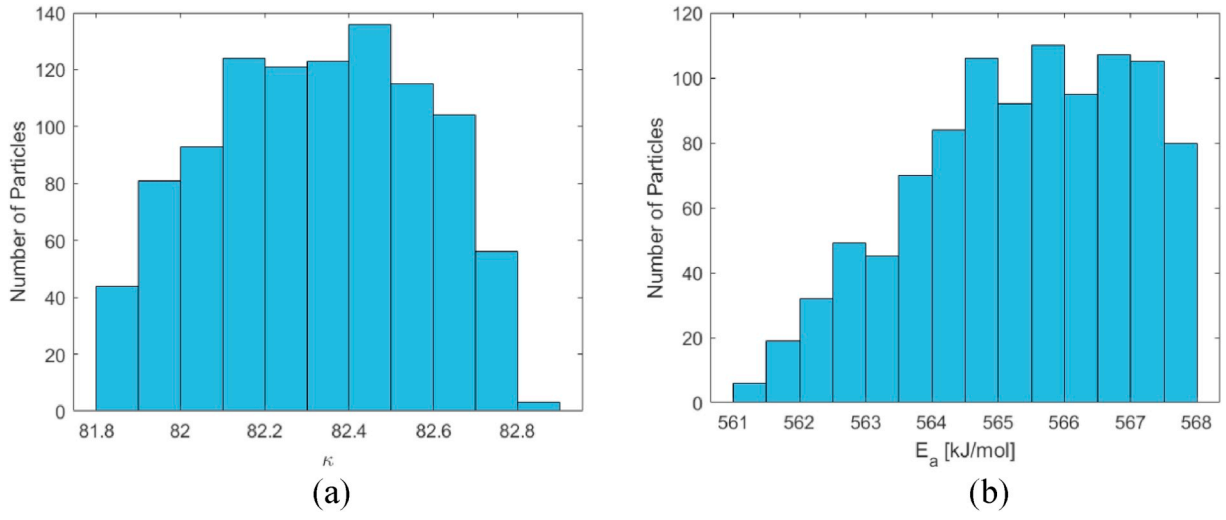

Fig. 6. Histograms for the parameters of Model 1 –. measurements generated with model 1: (a) κ (b) E_a.

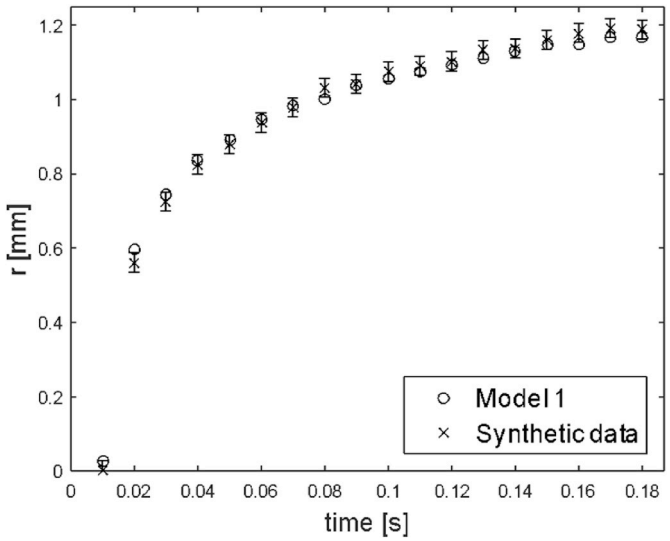

Fig. 7. Comparison between the synthetic data and the estimations –measurements generated with model 1.

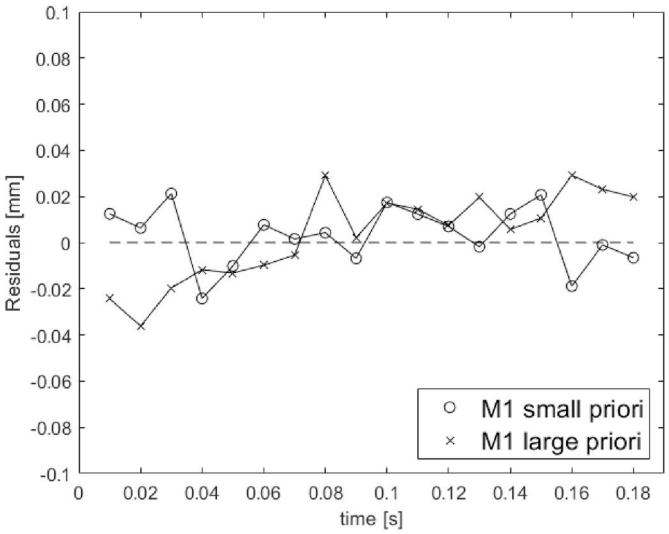

Fig. 9. Residuals obtained with priors of large and small variances – measurements generated with model 1.

Table 7
Statistics for the parameters of model 1 - measurements generated with model 1 and priors with small variances.

Parameters	Mean	Standard deviation	Quantile 2.5%	Quantile 97.5%
κ	35.0	0.8	33.5	36.2
E_a [kJ/mol]	232	6	221	240

deviations given by 1% of the exact transient front positions at the heated surface. For the solution of the inverse problem, both models were considered as equally probable, with uniform priors. The priors assumed for the model parameters were also uniform.

Despite the large uncertainties represented by the priors for the models and their corresponding parameters, the model used to generate the synthetic measurements was correctly selected for all test cases examined in this work. The model parameters were properly estimated when the measurements were generated with the two-state model. On the other hand, when the synthetic measurements were generated with the Arrhenius thermal damage model, the model parameters could only be correctly retrieved with priors of small variances. In fact, for a case which involved priors that encompassed values reported in the literature for different cell lines, parameters of the Arrhenius thermal damage model were not correctly estimated, despite that the agreement between estimated and measured necrosis front positions was qualitatively good. Therefore, parameter values reported in the literature for the Arrhenius thermal damage model need to be used with great caution, since different sets of values may result on the same thermal damage. The ABC algorithm used in this work provided the samples of the approximate posterior distribution of the model parameters at the final population, which were used for uncertainty quantification of the thermally affected region within the domain at the final time. The necrosis front positions predicted with a Monte Carlo simulation exhibited small variances and were centered around the exact values.

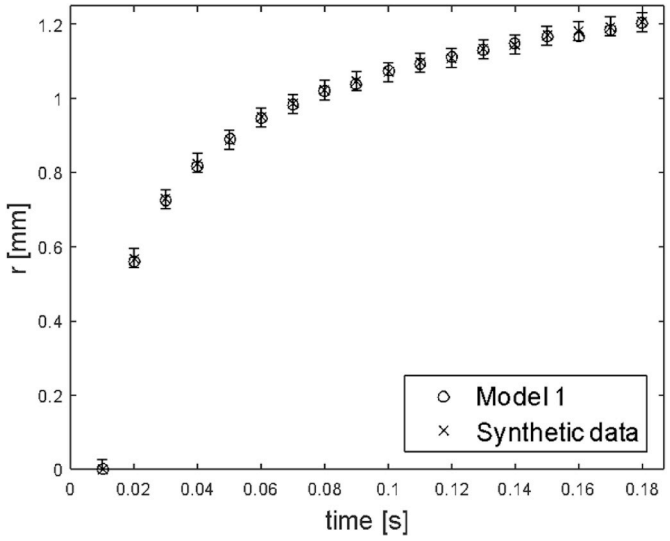

Fig. 8. Comparison between the synthetic data and the estimations –. measurements generated with model 1 and parameter priors with small variances.

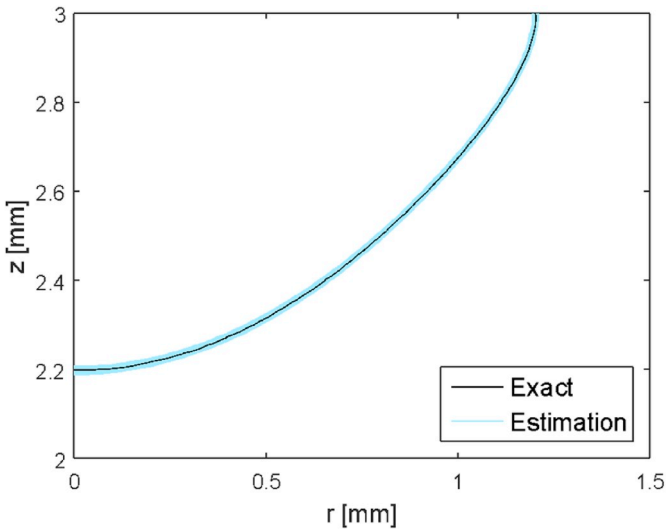

Fig. 10. Prediction of the necrosis front at the final time – measurements generated with model 1 and parameter priors with small variances.

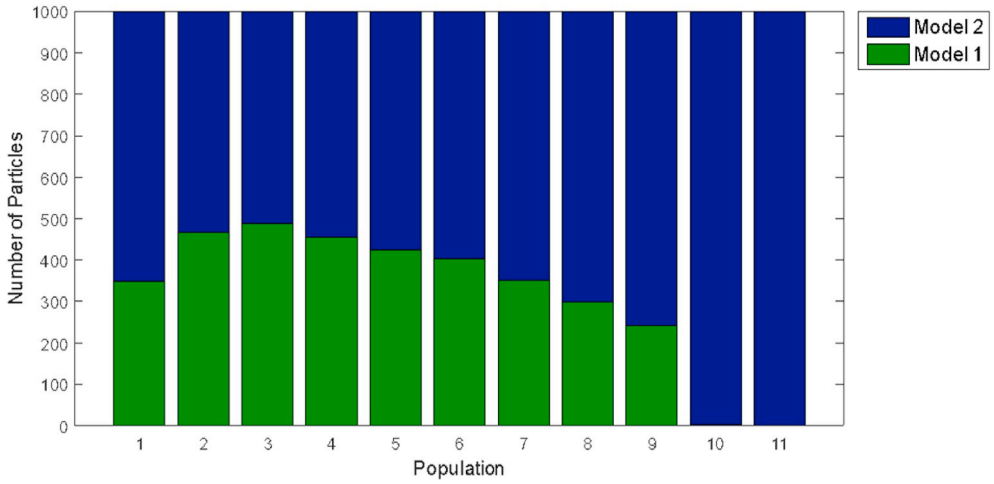

Fig. 11. Number of accepted particles at each population –. measurements generated with model 2.

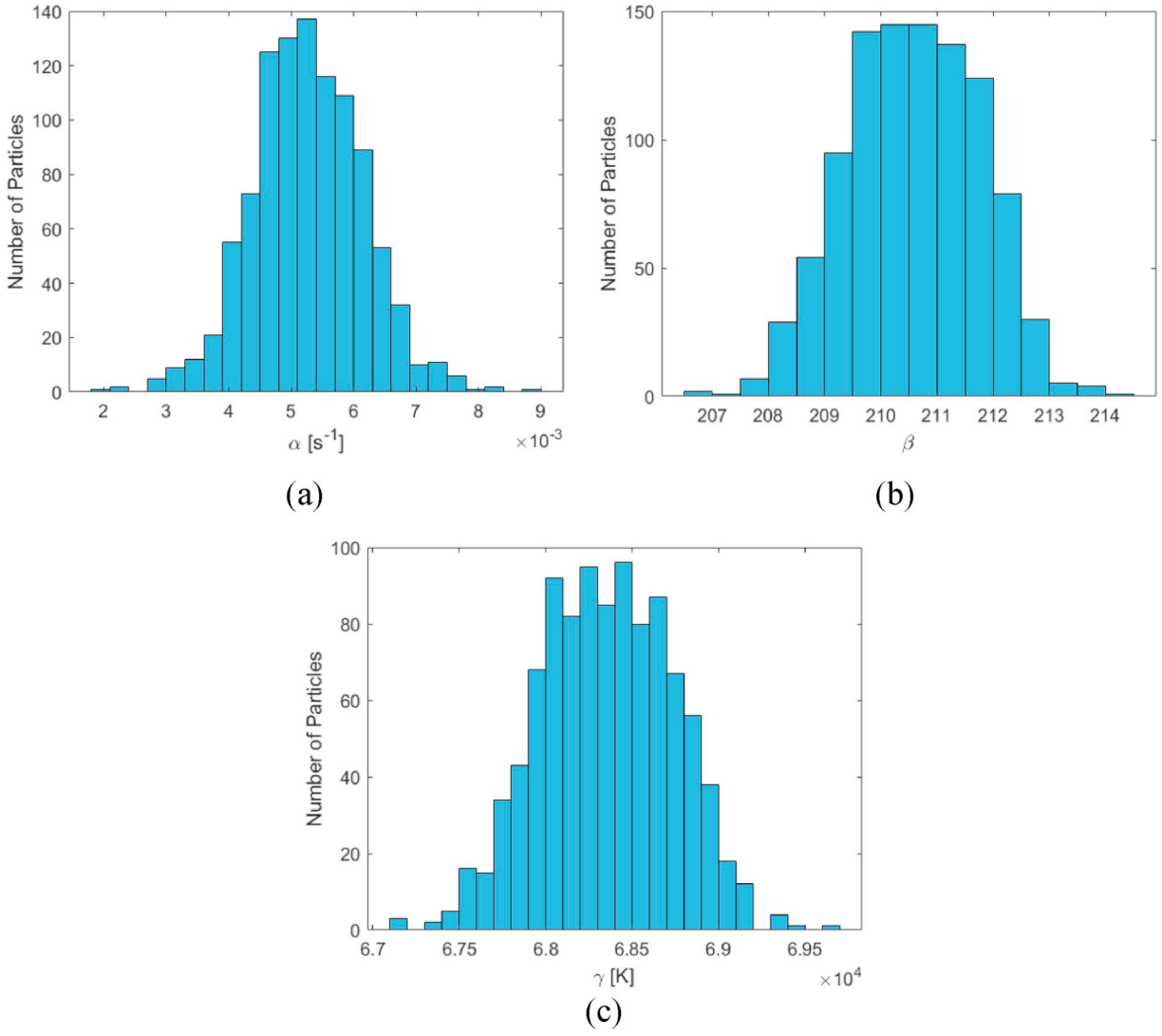

Fig. 12. Histograms for the parameters of model 2 –. measurements generated with model 2: (a) α; (b) β, (c) γ.

Table 8
Statistics for the parameters of model 2 –measurements generated with model 2.

Parameters	Mean	Standard deviation	Quantile 2.5%	Quantile 97.5%
α [s^{-1}]	0.0053	0.0009	0.0035	0.0071
β	211	1	208	213
γ [K]	68352	382	67593	69035

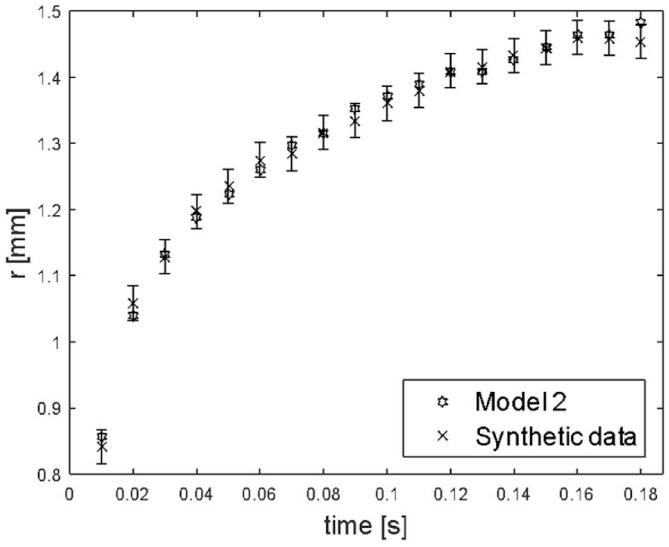

Fig. 13. Comparison between the synthetic data and the estimations - measurements generated with model 2.

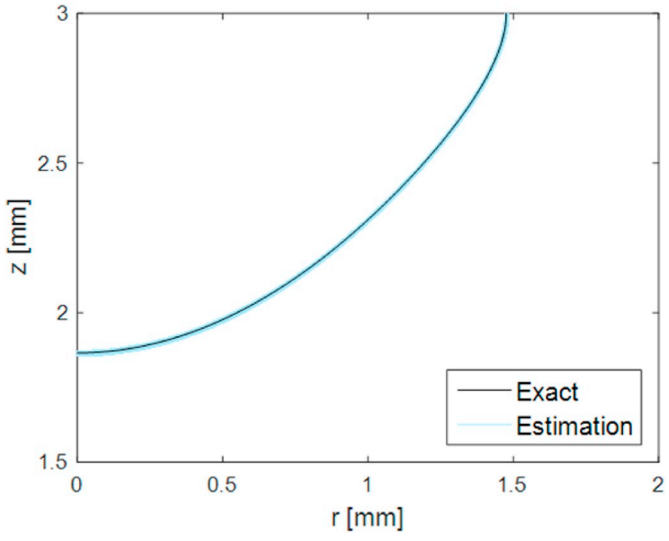

Fig. 14. Prediction of the necrosis front at the final time - measurements generated with model 2.

Author disclosure statement

There are no relationships of all authors with any people or organizations that could inappropriately influence (bias) this work.

Acknowledgements

The support provided by CNPq and FAPERJ, agencies of the Brazilian and Rio de Janeiro state governments, is gratefully appreciated. This study was financed in part by Coordenação de Aperfeiçoamento de Pessoal de Nível Superior - Brazil (CAPES) - Finance Code 001.

Appendix A. Supplementary data

Supplementary data to this article can be found online at https://doi.org/10.1016/j.ijthermalsci.2019.106243.

References

[1] J.V. Beck, K.J. Arnold, Parameter Estimation in Engineering and Science, John Wiley & Sons Inc, New York, 1977.
[2] H. Akaike, A new look at the statistical model identification, 1974, IEEE Trans. Autom. Control, Vol. 19(6), pp.716–723. DOI: 10.1109/TAC.1974.1100705.
[3] G. Schwarz, Estimating the dimension of a model, Ann. Stat. 6 (2) (1978) 461–464.
[4] A.N. Tikhonov, V.Y. Arsenin, Solution of Ill-Posed Problems, Winston & Sons, Washington, DC, 1977.
[5] P.C. Sabatier, Applied Inverse Problems: Lectures presented at the RCP 264 - Etude Interdisciplinaire des Problèmes Inverses, sponsored by the Centre National de la Recherche Scientifique, Springer, Berlin, 1978.
[6] G.S. Dulikravich (Ed.), Proceedings of the First International Conference on Inverse Design Concepts in Engineering Sciences (ICIDES-I), University of Texas, Dept. of Aero. Eng.& Eng. Mech., Austin, TX, College of Engineering, October .
[7] V.A. Morozov, Methods for Solving Incorrectly Posed Problems, Springer, New York, 1984.
[8] J.V. Beck, B. Blackwell, C.R. St Clair Jr., Inverse Heat Conduction: Ill-Posed Problems, Wiley Interscience, New York, 1985.
[9] G.S. Dulikravich (Ed.), Proceedings of the Second International Conference on Inverse Design Concepts and Optimization in Engineering Sciences (ICIDES-II), The Pennsylvania State University, University Park, PA, October 26–28, 1987.
[10] A. Tarantola, Inverse Problem Theory and Methods for Model Parameter Estimation, Society for Industrial and Applied Mathematics - SIAM, Philadelphia, 2005.
[11] G.S. Dulikravich (Ed.), Proceedings of the Third International Conference on Inverse Design Concepts and Optimization in Engineering Sciences (ICIDES-III)", Washington, D.C., October 23–25, 1991; Also NASA CR-188125, January 1992.
[12] E. Hensel, Inverse Theory and Applications for Engineers, Prentice Hall, New Jersey, 1991.
[13] G.S. Dulikravich, Aerodynamic shape design and optimization: status and trends, AIAA Journal of Aircraft 29 (5) (1992) 1020–1026, https://doi.org/10.2514/3.46279.
[14] D.A. Murio, The Mollification Method and the Numerical Solution of Ill-Posed Problems, Wiley Interscience, New York, 1993.
[15] O.M. Alifanov, Inverse Heat Transfer Problems, Springer, Berlin Heidelberg, 1994.
[16] O.M. Alifanov, E.A. Artyukhin, S.V. Rumyantsev, Extreme Methods for Solving Ill-Posed Problems with Applications to Inverse Heat Transfer Problems, Begell House, New York, 1995.
[17] G.S. Dulikravich, Shape Inverse Design and Optimization for Tree-Dimensional Aerodynamics, AIAA invited paper 95–0695, AIAA Aerospace Sciences Meeting, Reno, NV, USA, January 1995, https://doi.org/10.2514/6.1995-695.
[18] K. Kurpisz, A.J. Nowak, Inverse Thermal Problems, WIT Press, Southampton, UK, 1995.
[19] G.S. Dulikravich, Design and optimization tools development, in: H. Sobieczky (Ed.), New Design Concepts for High Speed Air Transport, Springer Wien/New York, 1997, pp. 159–236.
[20] D.M. Trujillo, H.R. Busby, Practical Inverse Analysis in Engineering, CRC Press, Inc, Boca Raton, FL, 1997.
[21] M. Bertero, P. Boccacci, Introduction to Inverse Problems in Imaging, Institute of Physics, London, UK, 1998.
[22] A.M. Denisov, Elements of the Theory of Inverse Problems, VSP, Utrecht, The Netherlands, 1999.
[23] A.G. Yagola, I.V. Kochikov, G.M. Kuramshina, Y.A. Pentin, Inverse Problems of Vibrational Spectroscopy, VSP, Utrecht, The Netherlands, 1999.
[24] M.N. Ozisik, H.R.B. Orlande, Inverse Heat Transfer: Fundamentals and Applications, Taylor and Francis, New York, 2000.
[25] K.A. Woodbury, Inverse Engineering Handbook, CRC Press, Boca Raton, 2002.
[26] J. Kaipio, E. Somersalo, Statistical and Computational Inverse Problems, Springer-, New York, 2004.
[27] M.J. Colaço, H.R.B. Orlande, G.S. Dulikravich, Inverse and optimization problems in heat transfer, J. Braz. Soc. Mech. Sci. Eng. 28 (1) (2006) 1–24.
[28] S. Tan, C. Fox, G. Nicholls, Inverse Problems, Course Notes for Physics 707, University of Auckland, 2006. https://sites.google.com/site/szemengtan/. (Accessed 13 December 2019).
[29] D. Calvetti, E. Somersalo, Introduction to Bayesian Scientific Computing, Springer, New York, 2007.
[30] H.R.B. Orlande, O. Fudym, D. Maillet, R.M. Cotta, Thermal Measurements and Inverse Techniques, CRC Press, Boca Raton, 2011.
[31] K. Farrell, J.T. Oden, D. Faghihi, A Bayesian framework for adaptive selection, calibration and validation of coarse-grained models of atomistic systems, J. Comput. Phys. 295 (2015) 189–208, https://doi.org/10.1016/j.jcp.2015.03.071.
[32] P. Del Moral, A. Doucet, A. Jasra, Sequential Monte Carlo for bayesian computation, Bayesian Statistics 8 (2007) 1–34.
[33] S.A. Sisson, Y. Fan, M.M. Tanaka, Sequential Monte Carlo without likelihoods, Proc. of the National Academy of Sciences of the USA 104 (6) (2007) 1760–1765, https://doi.org/10.1073/pnas.0607208104.

[34] T. Toni, D. Welch, N. Strelkowa, A. Ipsen, M.P.H. Stumpf, Approximate Bayesian computation scheme for parameter inference and model selection in dynamical systems, J. R. Soc. Interface 6 (2009) 187–202.
[35] T. Toni, M.P.H. Stumpf, Parameter inference and model selection in signaling pathway models, Computational Biology 673 (2010) 283–295, https://doi.org/10.1007/978-1-60761-842-3_18.
[36] T. Toni, M.P.H. Stumpf, Simulation-based model selection for dynamical systems in systems and population biology, Bioinformatics 26 (1) (2010) 104–110, https://doi.org/10.1093/bioinformatics/btp619.
[37] P. Del Moral, A. Doucet, A. Jasra, An adaptive sequential Monte Carlo method for approximate Bayesian computation, Stat. Comput. 22 (5) (2012) 1009–1020, https://doi.org/10.1007/s11222-011-9271-y.
[38] B.R. Loiola, H.R.B. Orlande, G.S. Dulikravich, Thermal damage during ablation of biological tissues, Numer. Heat Transf. A 73 (10) (2018) 685–701, https://doi.org/10.1080/10407782.2018.1464794.
[39] J.P. Abraham, E.M. Sparrow, A thermal-ablation bioheat model including liquid-to-vapor phase change, pressure- and necrosis-dependent perfusion, and moisture-dependent properties, Int. J. Heat Mass Transf. 50 (2007) 2537–2544, https://doi.org/10.1016/j.ijheatmasstransfer.2006.11.045.
[40] F.C. Henriques Jr., Studies of thermal injury V. The predictability and the significance of thermally induced rate processes leading to irreversible epidermal injury, Arch. Pathol. 43 (5) (1947) 489–502.
[41] F.C. Henriques Jr., A.R. Moritz, Studies of thermal injury I. The conduction of heat to and through skin and the temperatures attained therein: a theoretical and an experimental investigation, Am. J. Pathol. 23 (4) (1947) 531–549.
[42] A.R. Moritz, Studies of thermal injury III. The pathology and pathogenesis of cutaneous burns: an experimental study, Am. J. Pathol. 23 (6) (1947) 915–941.
[43] A.R. Moritz, F.C. Henriques Jr., Studies of thermal injury II. The relative importance of time and surface temperature in the causation of cutaneous burns, Am. J. Pathol. 23 (5) (1947) 695–720.
[44] J.A. Pearce, Comparative analysis of mathematical models of cell death and thermal damage processes, Int. J. Hyperth. 29 (4) (2013) 262–280, https://doi.org/10.3109/02656736.2013.786140.
[45] Y. Feng, J.T. Oden, M.N. Rylander, A two-state cell damage model under hyperthermic conditions: theory and in vitro experiments, J. Biomech. Eng. 130 (4) (2008), 041016, https://doi.org/10.1115/1.2947320.
[46] B. Lamien, H.R.B. Orlande, L.A.B. Varón, R.L.Q. Basto, G.E. Eliçabe, D.S. Santos, R. M. Cotta, Estimation of the temperature field in laser-induced hyperthermia experiments with a phantom, Int. J. Hyperth. 35 (2018) 279–290, https://doi.org/10.1080/02656736.2018.1496283.
[47] T.E. Cooper, G.J. Trezek, Correlation of thermal properties of some human tissues with water content, Aero. Med. 42 (1) (1971) 24–27.
[48] H.H. Pennes, Analysis of tissue and arterial blood temperatures in the resting human forearm, J. Appl. Physiol. 1 (2) (1948) 93–122, https://doi.org/10.1152/jappl.1948.1.2.93.
[49] J.H. Lambert, Photometry or On the Measure and Gradations of Light, Color, and Shade. Translate from Photometria sive de mensura et gradibus luminis, colorum et umbrae by David L. DiLaura, Augsburg, Illuminating Engineering Society, 2001.
[50] J.A. Pearce, I.F. Çilesiz, A.J. Welch, E.K. Chan, T.J. McMurray, S.L. Thomsen, Comparison of Ho:YAG, Tm:YAG and Argon lasers for fusion of intestinal tissues, Proc. SPIE Laser Surgery: Advanced Characterization, Therapeutics, and Systems IV 2128 (1994) 517–526, https://doi.org/10.1117/12.184938.
[51] S.L. Jacques, S.A. Prahl, Modeling optical and thermal distributions in tissue during laser irradiation, Lasers Surg. Med. 6 (6) (1987) 494–503, https://doi.org/10.1002/lsm.1900060604.
[52] M.A. Beaumont, W. Zhang, D.J. Balding, Approximate bayesian computation in population genetics, Genetics 162 (4) (2002) 2025–2035.
[53] P. Marjoram, J. Molitor, V. Plagnol, S. Tavaré, Markov chain Monte Carlo without likelihoods, Proc. of the National Academy of Sciences of the USA 100 (26) (2003) 15324–15328, https://doi.org/10.1073/pnas.0306899100.
[54] D. Wegmann, C. Leuenberger, L. Excoffier, Efficient approximate bayesian computation coupled with Markov chain Monte Carlo without likelihood, Genetics 182 (4) (2009) 1207–1218, https://doi.org/10.1534/genetics.109.102509.
[55] S.V. Patankar, Numerical Heat Transfer and Fluid Flow, Hemisphere Publishing Corporation, Washington, 1980.
[56] M.N. Ozisik, H.R.B. Orlande, M.J. Colaço, R.M. Cotta, Finite Difference Methods in Heat Transfer, second ed., CRC Press, Boca Raton, 2017.
[57] M.J. Moran, H.N. Shapiro, Fundamentals of Engineering Thermodynamics, fifth ed., John Wiley & Sons, Inc., England, 2006.
[58] H.H. Mitchell, T.S. Hamilton, F.R. Steggerda, H.W. Bean, The chemical composition of the adult human body and its bearing on the biochemistry of growth, J. Biol. Chem. 158 (1945) 625–637.
[59] T.L. Bergman, A.S. Lavine, F.P. Incropera, D.P. DeWitt, Fundamentals of Heat and Mass Transfer, seventh ed., John Wiley & Sons, Inc, US, 2011.
[60] S.L. Thomsen, J.A. Schwartz, R. Joseph, J.A. Pearce, B. Rae, T.J. McMurray, Temperatures associated with thermally induced red blood cell changes in tissues irradiated in vivo, Proc. SPIE 2130 (1994) 156–163, https://doi.org/10.1117/12.179925.
[61] A.J. Welch, M.J.C. van Gemert, Optical-Thermal Response of Laser-Irradiated Tissue, second ed., Springer Science+Business Media B.V, 2011.
[62] C.A. Linte, J.J. Camp, M.E. Rettmann, D. Haemmerich, M.K. Aktas, D.T. Huang, D. L. Packer, D.R. Holmes III, Lesion modeling, characterization, and visualization for image-guided cardiac ablation therapy monitoring, J. Med. Imaging 5 (2018), 021218, https://doi.org/10.1117/1.JMI.5.2.021218.